

Comprehensive investigation of sequential plasma activated Si/Si bonded interfaces for nano-integration on the wafer scale

M G Kibria¹, F Zhang¹, T H Lee², M J Kim² and M M R Howlader¹

¹ Department of Electrical and Computer Engineering, McMaster University,
1280 Main Street West, Hamilton, ON, L8S 4K1, Canada

² Department of Materials Science and Engineering, University of Texas at Dallas,
TX 75080, USA

E-mail: kibriamg@mcmaster.ca and mrhowlader@ece.mcmaster.ca

Received 15 August 2009, in final form 3 November 2009

Published 8 March 2010

Online at stacks.iop.org/Nano/21/134011

Abstract

The sequentially plasma activated bonding of silicon wafers has been investigated to facilitate the development of chemical free, room temperature and spontaneous bonding required for nanostructure integration on the wafer scale. The contact angle of the surface and the electrical and nanostructural behavior of the interface have been studied. The contact angle measurements show that the sequentially plasma (reactive ion etching plasma followed by microwave radicals) treated surfaces offer highly reactive and hydrophilic surfaces. These highly reactive surfaces allow spontaneous integration at the nanometer scale without any chemicals, external pressure or heating. Electrical characteristics show that the current transportation across the nanobonded interface is dependent on the plasma parameters. High resolution transmission electron microscopy results confirm nanometer scale bonding which is needed for the integration of nanostructures. The findings can be applied in spontaneous integration of nanostructures such as nanowires/nanotubes/quantum dots on the wafer scale.

(Some figures in this article are in colour only in the electronic version)

1. Introduction

Wafer bonding refers to the process of joining clean and mirror-polished smooth (rms surface roughness less than 0.5 nm) surfaces. It is one of the key process steps in the fabrication of silicon-on-insulator (SOI) substrates, in three-dimensional integration of microelectromechanical systems (MEMS), and in the fabrication of optoelectronic and photonic devices [1]. Recently, wafer bonding has gained remarkable attention for creating nanoscale devices such as carbon nanotube (CNT) based MEMS (i.e. microcoolers) [2] and ordered templates to realize self-assembly of molecules, nanowires (NWs) or quantum dots (QDs) [3, 4]. To bond these nanostructures (i.e., CNTs, NWs, QDs), current wafer bonding methods utilize wet chemical processes, high temperature annealing steps and external forces to achieve high bonding strength. A number of studies on integration of nanostructures have been reported using diffusion, adhesive, chemical, ultrasonic vibrational force, thermocompression and

electrothermal bonding methods [5–9]. The issues in these methods are: (1) high bonding temperature and external force may not be suitable for bonding nanostructures due to their delicate nature, (2) adhesive bonding results in reduced current transport and reduced mechanical stability, (3) the wet chemical processes before bonding may not be applicable for bonding chemically sensitive delicate materials with substrates that contain metals. In addition, the high temperature annealing steps after bonding can modify the doping profile, and generate large threading and misfit dislocations in heterogeneously bonded nanostructures that have different thermal expansion coefficients and a large lattice mismatch [10].

To address all the above issues, we have developed a bonding process called sequential plasma activated bonding (SPAB). This bonding method does not require any wet chemicals, intermediate adhesives, external forces and annealing steps to achieve high bonding strength [11] even for the integration of dissimilar materials with large lattice mismatch. For sequential activation, the surfaces are treated

using oxygen (O_2) reactive ion etching (RIE) plasma followed by nitrogen (N_2) microwave (MW) radicals. This treatment is called surface activation, which removes contaminants (i.e. hydrocarbon and metal ions from tweezers), native oxides (i.e. SiO_2 in the case of silicon (Si)), and particles from the surfaces. The treatment leads to the formation of new hydroxyl (OH^-) groups on the treated surface, making the surface easier to wet with water; thus the treatment makes it a hydrophilic surface. The higher the degree of hydrophilicity, the easier it is to do bonding at room temperature [1]. This results in spontaneous bonding at low temperature, which is required for nanostructure integration. The bonding strength achieved through SPAB without post-bonding annealing is equivalent to the bulk fracture strength of the mating wafers [11, 12]. The high bonding strength achieved through SPAB allows thinning down one of the bonded wafers to an ultrathin film a few nanometers thick. This thin film can be used to fabricate nanofilters for trapping biological species, such as yeast cells and bacteria [13]. It has been reported that Si NW bridges can be grown between two vertical silicon sidewalls [14]. Nanoscale bonding between the nanofilters and the Si NW bridges allows creating nanoscale sensing devices for biomedical applications.

As previously mentioned, the bonded interface properties largely depend on surface hydrophilicity before bonding [1]. However, there are no reported results currently on sequentially plasma activated surface hydrophilicity, which ultimately determines the spontaneous bonding strength. In addition, the bonded structures may go through post-bonding annealing steps in real applications, such as in Smart Cut[®] technology to transfer thin layers [15], which may change the interfacial morphology. Furthermore, current transport across the bonded interface is a major concern for nanoscale device design, especially for near-surface interfaces [16]. Although a significant number of reports have been aimed at the electrical characterization of only O_2 RIE plasma activated and chemically activated Si/Si bonded interfaces [17–19], no reports have been published yet on the electrical characterization of sequentially plasma activated Si/Si bonded interfaces. This characterization of the bonded interface provides a scientific basis for integration of nanostructures on whole wafers [20] that is required for mass production of nanoscale devices.

This paper reports the following:

- (1) An in-depth analysis of hydrophilicity of Si wafers using contact angle measurements to figure out how sequential plasma activates surfaces for spontaneous bonding at the nanometer scale.
- (2) An extensive investigation of electrical conductivity of the nanobonded interface using direct current–voltage (I – V) measurements with different plasma parameters and annealing temperatures
- (3) A demonstration of the nanobonded interfaces after annealing at different temperatures using high resolution transmission electron microscopy (HRTEM) and electron energy loss spectroscopy (EELS).

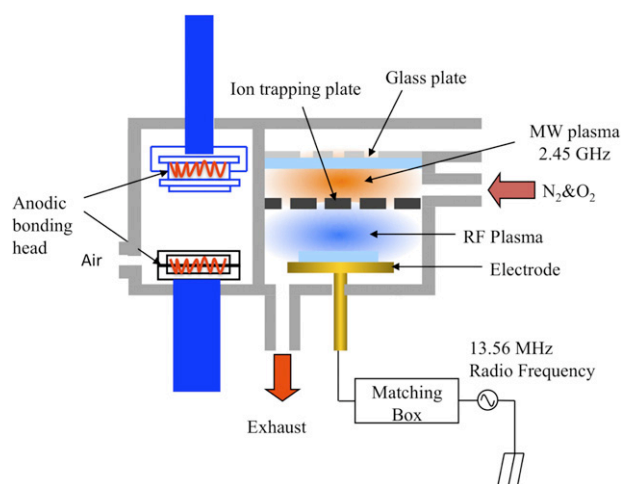


Figure 1. Hybrid plasma bonding system.

2. Experiments

2.1. Specimens

Commercially available Czochralski (CZ) grown one-side-polished 4 in p-type (100) oriented Si wafers were used for experiments. The thicknesses of the wafers were $525 \pm 25 \mu\text{m}$ and the resistivity was between 0.1 and 100 $\Omega \text{ cm}$.

2.2. The hybrid plasma bonding system and activation procedure

The surface activation and wafer bonding were accomplished using a wafer level hybrid plasma bonding (HPB) system, which was developed based on the sequential plasma activation and anodic bonding techniques, as shown in figure 1. It consists of plasma activation and anodic bonding chambers. In the sequential plasma activation process, the wafer surfaces are sequentially activated by a radio frequency (RF) reactive ion etching (RIE) plasma with high bombardment energy followed by microwave (MW) plasma of neutral radicals with high reactivity. The RIE plasma removes contaminations from the surface by a physical sputtering mechanism, whereas the MW neutral radical creates chemically unstable wafer surfaces. The plasma activation chamber is separated into top and bottom compartments by means of an ion trapping metallic plate. Using the ion trapping metallic plate, neutral radicals are produced at the bottom compartment. The bottom and top sides of the chamber were used to generate RIE and MW plasma from O_2 and N_2 gases, respectively. For the experiments presented here, only the plasma activation chamber was used. The anodic bonding chamber is only required to perform the anodic bonding of wafers. Details of the sequential plasma activation system can be found elsewhere [11].

The wafer surfaces were activated by a sequential plasma activation process in the plasma activation chamber at a low vacuum. To activate the wafers, the as received wafers were placed into the plasma activation chamber. Then, the wafers were activated using O_2 RIE plasma at a frequency of 13.56 MHz. The O_2 plasma parameters include an oxygen

flow rate of 50 sccm, RF power varied from 100 to 400 W, chamber pressure varied from 40 to 250 Pa, and the plasma treatment time varied from 5 to 300 s. Lastly, the RIE plasma treated wafers were further processed using electrically neutral ions from N₂ MW radical plasma generated at a frequency of 2.45 GHz. The MW radical parameters include a nitrogen flow rate of 50 sccm, power 2000 W, chamber pressure 100 Pa, and plasma treatment time 30 s. With these plasma parameters, the bias voltage at the substrate electrode varied between -35 and -185 V.

2.3. Other experiments

After plasma activation, the wafers were taken out of the chamber, and the contact angle was measured using the sessile drop method with a deionized (DI) water droplet (9 μ l). The Kruss drop shape analysis system DSA10 was used to measure the contact angle. A contact angle below 2° cannot be detected using the equipment. A separate set of wafers were bonded together using hand applied pressure immediately after plasma activation, and then investigated using current-voltage (*I-V*) measurement, and high resolution transmission electron microscopy (HRTEM). Highly conductive silver paste (typical resistivity $\sim 3 \times 10^{-5} \Omega \text{ cm}$) was used to make contact electrodes with the bonded wafer for *I-V* characterization. Metal electrodes were not chosen because of the possibility of sintering the electrode metal and silicon at high annealing temperatures [21]. Before annealing, the silver electrodes were removed. An HP-4145B Semiconductor Parameter Analyzer was used for *I-V* characterization. For the temperature dependent electrical characterization and HRTEM, the bonded wafer pieces were annealed following a predefined annealing profile which will be discussed later. Specimens for HRTEM were prepared from the bonded pairs by standard procedures including polishing, dimpling, and ion-milling. To investigate the elemental composition at the bonded interface, electron energy loss spectroscopy (EELS) was performed.

3. Results and discussion

3.1. Contact angle measurements

A straightforward way to study surface hydrophilicity is to measure the contact angle of a drop of water on the surface. The lower the contact angle, the higher the degree of hydrophilicity, resulting in better wettability of the surface. This is critical for this study since the higher the surface hydrophilicity, the easier it is to bond between the surfaces [22]. Figure 2 shows the contact angle (β) of a drop of DI water on an Si wafer surface. The contact angle is related to the surface energy of the solid and the surface tension of the liquid by the Young equation [23], as

$$\gamma_{\text{sg}} - \gamma_{\text{sl}} - \gamma_{\text{g}} \cos \beta = 0. \quad (1)$$

The liquid-gas interface energy γ_{g} (i.e. surface tension) and the solid-liquid interface energy γ_{sl} depend on the liquid being used. The solid-gas interface energy γ_{sg} , also called the solid surface energy, increases with a decrease in contact

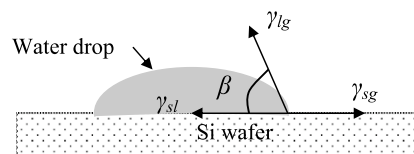


Figure 2. Schematic of a droplet of water on an Si wafer surface and the contact angle β .

angle. For hydrophilic surfaces, the contact angle usually remains much less than 45°, and it is usually higher than 45° for hydrophobic surfaces [15]. Hence, a hydrophilic surface is easier to bond than a hydrophobic surface.

In order to understand the influence of different plasma parameters associated with sequential activation on the degree of hydrophilicity (i.e., surface energy), the contact angle measurements were carried out with different O₂ RIE plasma parameters (e.g., time, power and pressure). Similar measurements using N₂ MW radical parameters will be reported later. Recently the hydrophilicities of Si and Ge wafer surfaces were investigated after O₂ and N₂ RIE plasma activation [22]. Although the authors [22] recommended wafer bonding immediately after plasma activation, the contact angle measurements were done within 2 h after plasma activation. In this study, the surface hydrophilicity was investigated through contact angle measurements after three minutes of plasma activation in order to understand the applicability of SPAB, especially in bonding and packaging environments where a few minutes may be required for handling and alignment after surface activation.

The average measured contact angles at different plasma processing conditions are listed in table 1. It also includes the average contact angles of non-activated surface, and hydrophobic surfaces cleaned with diluted (5%) hydrofluoric (HF) acid for comparison. The contact angles of the sequentially activated surface show an increasing trend as the O₂ RIE plasma activation time, power and pressure increase. This result can be correlated with the surface roughness, which has been reported to increase with O₂ RIE plasma parameters such as activation time and power [24]. Rough surfaces are known to have a higher contact angle compared to that of smooth surfaces [25]. Hence, increasing the surface roughness with O₂ RIE plasma parameters in a sequential plasma activation process can increase the contact angle. Furthermore, the physical bombardment process of O₂ RIE plasma removes surface species such as contaminations, carbons, hydrogen, hydroxyl (OH⁻) groups, and it creates large numbers of free bonds (dangling bonds) on the surface. It is well known that the more OH⁻ groups present on the surface, the smaller the contact angle. Increasing the plasma power, pressure, and time enhances the physical bombardment process of O₂ RIE and removes surface OH⁻ groups more efficiently; thus, this increases the contact angle. It is important to note that the plasma activation was performed on a silicon wafer surface that is covered with a few nanolayers of native oxide. In fact, O₂ RIE treatment not only removes surface contaminations, but also produces a plasma induced oxide layer. However, the thickness of this oxide layer does not make

Table 1. The average contact angles of a drop of DI wafer on an Si wafer surface with different surface treatment conditions.

O ₂ RIE plasma			N ₂ MW radical			Contact angle (deg)
Pressure (Pa)	Power (W)	Time (s)	Pressure (Pa)	Power (W)	Time (s)	
100	300	5	100	2000	30	31.4 ± 1.1
		15				36.8 ± 0.5
		30				38.1 ± 0.5
		60				39.5 ± 0.3
		120				37.7 ± 0.5
	300					40.6 ± 0.3
100	50	60	100	2000	30	34.5 ± 0.7
	75					31.5 ± 0.3
	100					38.8 ± 0.6
	200					39.5 ± 0.3
	300					39.5 ± 0.3
	400					43.1 ± 0.5
40	300	60	100	2000	30	38.5 ± 0.5
60						41.0 ± 1.3
80						39.4 ± 0.2
100						39.5 ± 0.3
120						40.1 ± 1.0
Without activation						33.4 ± 0.2
HF cleaning (5%)						65.2 ± 0.4
RCA cleaning (H ₂ O:H ₂ O ₂ :NH ₄ OH = 5:1:1)						9.9 ± 0.4
Only O ₂ RIE activation (100 Pa, 300 W, 30 s)						43.0 ± 0.4
Only N ₂ MW activation (100 Pa, 2000 W, 30 s)						26.1 ± 2.3

a significant difference in contact angle and hence surface energy as reported in [22].

When we manipulated with the O₂ RIE plasma power, the lowest contact angle that we could achieve was at 75 W. The plasma power at 50 W was not sufficient to activate the wafer surfaces, which resulted in a contact angle near to that of a non-activated surface. It can be concluded from the above results that lowest contact angles can be achieved by choosing the lowest possible O₂ RIE plasma parameters. However, the plasma parameters have to be high enough to sufficiently remove surface contaminations and activate the surface. Our experimental results show that the lowest possible O₂ RIE parameters that can sufficiently activate the surface are 5 s, 75 W, and 40 Pa. It has been reported that the surface roughness is less than 0.5 nm at these plasma parameters, and hence suitable for wafer bonding [26, 27].

To clarify the relative influence of O₂ RIE plasma and N₂ MW radicals, the contact angle measurements were carried out after treating the wafers with O₂ RIE plasma and N₂ MW radicals separately. The results (table 1) indicate that the hydrophilicity of a silicon wafer treated with N₂ MW radical is better compared to that when it is treated with O₂ RIE plasma. The N₂ MW radicals do not physically bombard the surface. This is because the N₂ MW radical is not accelerated by the DC self-bias voltage. The surface treated only with N₂ MW is unstable, resulting in a high deviation in contact angle as high as about 10% (table 1). The N₂ MW radical neither removes surface OH⁻ groups and other contaminations nor reduces surface hydrophilicity. The unique behavior of the N₂ MW radical can be explained as follows. The N₂ MW radical is highly reactive, resulting in silicon oxynitride (SiO_xN_y) and Si–N bonds while reacting with oxygen and silicon [28]. These

bonds control the water contact angles that largely depend on two factors, dispersion γ^d and polar γ^p components, which determine the surface energy. The higher the polar contribution (γ^p) to the surface energy, the better the wettability of a polar liquid like water [29]. While the presence of Si–N bonds on the N₂ MW radical treated surface leads to a higher polar contribution, the presence of Si–O bonds on the O₂ RIE treated surface results in a lower polar contribution to the surface energy [30]. Hence, the N₂ MW radical activated surface is much more hydrophilic than the O₂ RIE plasma activated surface.

Immediately after plasma activation, silicon wafer surfaces are terminated by large numbers of dangling bonds, and they can react with the surrounding environment, such as water, impurity components, or with other dangling bonds. To clarify the ageing process of the surface, a droplet of DI water was placed on an Si wafer surface and the contact angles were measured after every 3 s. Figure 3 depicts the contact angles as a function of exposure time in air after sequential activation compared with O₂ RIE plasma activation, N₂ MW radical activation, diluted (5%) HF cleaning, and the contact angles of the non-activated surface. For sequential activation the O₂ RIE parameters were 300 W, 100 Pa and 15 s and the N₂ MW parameters were 2000 W, 100 Pa and 30 s. The plasma parameters for only O₂ RIE and only N₂ MW activation are given in table 1. The measurement errors associated with this experiment were ±10%. While the contact angle of HF cleaned and without activated wafer surface slowly decreased over time, the contact angle of the plasma activated surfaces decreased rapidly over time. The contact angle for the N₂ MW treated surface went below the detection limit within 176 s. The rate of change of the contact angle refers to

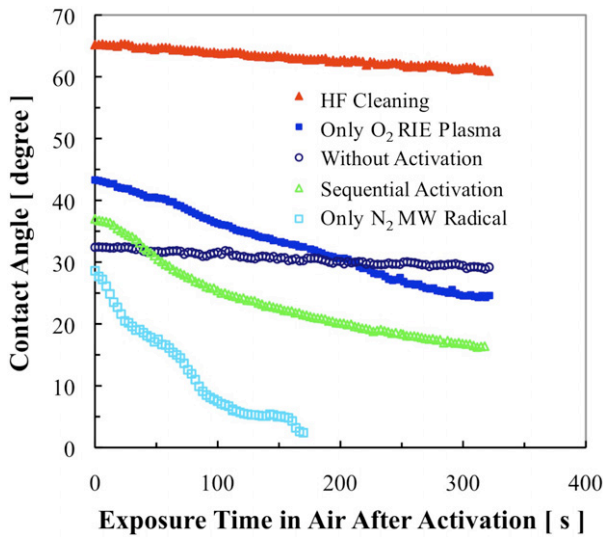


Figure 3. Contact angles of a droplet of DI water on an Si wafer surface. Contact angles were measured every 3 s starting from three minutes after plasma activation.

surface reactivity. This indicates that the N₂ MW radical treated surface is highly reactive. The highly reactive nature of N₂ MW radicals turns the sequentially activated surfaces into high reactive surfaces, in contrast to the HF treated surface and the non-activated surface. On the other hand, the contact angles of O₂ RIE treated surfaces were higher than those of N₂ MW treated surfaces and sequentially activated surfaces. The contact angles of sequentially plasma activated surfaces were less than those of O₂ RIE plasma treated surfaces but greater than those of N₂ MW radical activated surfaces throughout the elapsed time. As mentioned previously, O₂ RIE is required to remove surface contaminations and N₂ MW is required to create a highly reactive surface. Hence, both plasmas are essential to activate the surface for bonding. The decrease of the contact angle (i.e., increase in surface energy) over the storage time may be correlated with the increase of the bonding strength over the storage time. It has been reported that the bonding energy of sequentially plasma activated Si/Si interfaces significantly increases from ~0.05 to 2.3 J m⁻² after storage at RT for 24 h [31]. Increasing the elapsed time generates stronger bonds between the sequentially treated surfaces as a result of SiO_xN_y or Si–N. A similar mechanism in the reduction of the contact angle of the sequentially activated surface left in the air also explains the increase in surface energy due to SiO_xN_y or Si–N structures.

3.2. Electrical characterization of bonded interfaces

3.2.1. The influence of the plasma exposure time. The influence of the plasma processing parameters on the electrical characteristics of the bonded interface was investigated using *I–V* measurements. Figure 4 shows the *I–V* curves of the p-Si/p-Si bonded interface with different O₂ RIE plasma exposure times measured at RT. It has been reported [5] that sequential plasma activated wafers form covalent bonds across the bonded interface 24 h after bonding. Hence, the *I–V* measurements were done 24 h after bonding. After 24 h, no

significant change in *I–V* characteristics with storage time was found. From figure 4 it is evident that the electrical resistance increased as the O₂ RIE plasma activation time increased. The slow turn on of the forward and reverse bias currents indicates that a thin barrier layer is present at the bonded interface [32]. The experimental measurement of the oxide thickness on the O₂ RIE plasma activated silicon surfaces showed that the initial high oxide growth rate saturated at around 60 Å after approximately 100 s of plasma activation [33]. This result can be directly correlated with the electrical behavior shown in figure 4. It is seen that the positive bias current saturates after approximately 100 s of plasma activation time.

The electrical resistance at an arbitrarily chosen voltage of 4 V for 30 s of plasma activation time was calculated to be 778.4 kΩ. This high resistance is attributed to the presence of plasma induced charges and extra energy states at the bonded interface and at the band gap of the semiconductor, respectively. This was confirmed with the nonlinear *I–V* characteristics in figure 4. The presence of charges at the Si/Si bonded interface was also confirmed by a transient current response to a step voltage [34]. It has been reported that the O₂ RIE plasma activation can increase the fixed oxide charge by $2.9 \times 10^{10} \text{ cm}^{-2}$ and the interface trap density to $7.2 \times 10^{10} \text{ cm}^{-2} \text{ eV}^{-1}$ [35]. These oxide charges form a depletion region surrounding the bonded interface. The fixed oxide charges and interface traps generate extra energy states at the forbidden energy gap; which increase the barrier height at the bonded interface. This energy barrier hinders the flow of the majority carriers at the conduction band of the semiconductor, and thus results in high electrical resistance. Since the barrier height follows the same trend as the oxide thickness across the bonded interface [33], the oxide thickness has a dominant role in increasing the interface resistance.

For p-type silicon, positive charges form at the bonded interface that is balanced by negatively charged ionized acceptor atoms at the depletion region. A schematic energy band diagram of p-Si/p-Si is shown in figure 5. For lower doping ($\leq 10^{17} \text{ cm}^{-3}$) concentration, the current transport is dominated by the thermionic emission current. Using the thermionic emission model, the current density can be expressed as [36, 37]

$$J = A^* T^2 \exp\left(-\frac{qV_b}{kT}\right) \left[\exp\left(\frac{qV_2}{nkT}\right) - \exp\left(-\frac{qV_1}{nkT}\right) \right] \quad \text{and} \quad V = V_1 + V_2 \quad (2)$$

where A^* is the effective Richardson constant, T the temperature, q the electronic charge, k the Boltzmann constant, V_b the barrier height and n the ideality factor. V is the total applied bias, which is distributed over the interface with V_1 and V_2 components as shown in figure 5. The barrier height can be determined from the *I–V* characteristics in the forward direction with $V > 3kT/q$,

$$V_b = \frac{kT}{q} \ln\left(\frac{AT^2}{J_0}\right) \quad (3)$$

where J_0 is the extrapolated value of the current density at zero voltage. Assuming $A^* = 114 \text{ A cm}^{-2} \text{ K}^{-2}$ and

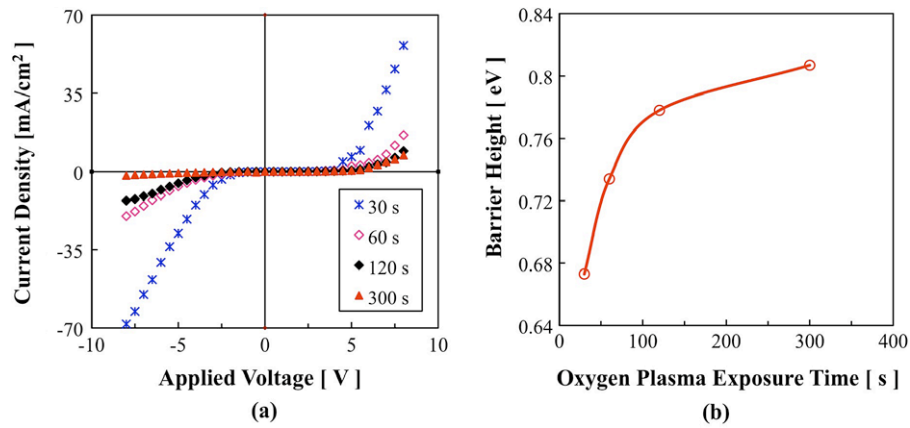


Figure 4. (a) Current–voltage characteristics of the bonded interface as a function of O₂ RIE plasma activation time. (b) Barrier height as a function of O₂ RIE plasma exposure time.

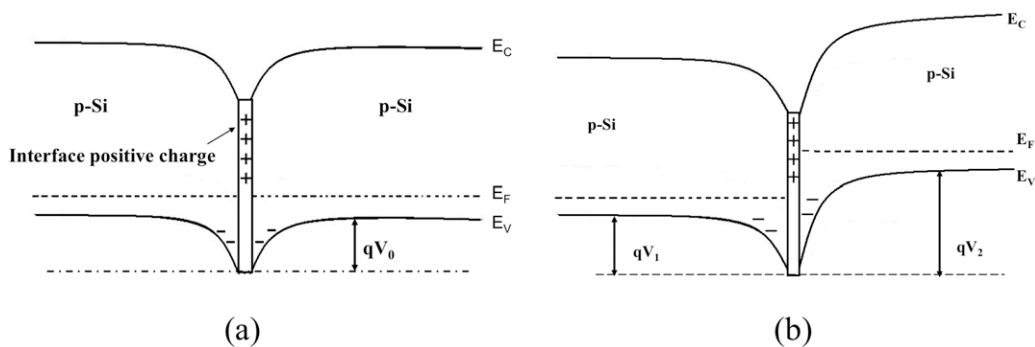


Figure 5. Schematic energy band diagram of a p-Si/p-Si bonded structure with (a) zero bias, (b) applied bias.

$T = 300$ K, the barrier height was determined and it is plotted in figure 4(b). The barrier height increased with the increase of the O₂ RIE plasma time. The slope of the barrier height from 30 to 120 s is higher than it is from 120 to 300 s. The barrier height at 300 s almost looks saturated. The increase in barrier height with the increase in O₂ RIE plasma time can be attributed to the increase in oxide thickness at the bonded interface [33]. The calculated barrier height of the bonded interface is higher than that of the chemically activated hydrophilic bonded interface [17]. This is attributed to the contact resistance between silver paste and silicon, and the plasma induced crystalline defects and interface fixed charges [38]. In fact, this additional contribution to the barrier height can be neglected for this comparative study. From the above results, it can be concluded that the current transport across the bonded interface can be controlled by a proper choice of the O₂ RIE plasma activation time.

3.2.2. The influence of the post-bonding annealing. The analysis of the electrical characteristics of the bonded interface upon post-bonding annealing allows us to further understand the defects and interface states and charges. It has been reported that the density of the interface states changes with the lateral positions of the bonded pair [17]. To avoid this issue, a single bonded pair with 10×10 mm² dimension was used for the I – V measurement at different temperatures

instead of four different bonded pairs. The I – V characteristics of the bonded pair were measured at room temperature without annealing and this was followed by annealed measurements at 200, 400, and 600 °C, respectively. At each temperature step, the electrodes were removed before annealing. Each time an annealing process was completed, the specimen was cooled and the I – V curves were measured accordingly. The ramping rate was kept constant at 200 °C h⁻¹, and the bonded pair was annealed for 4 h in air at all three temperature steps. For the sequential activation, the wafer surfaces were processed by a 200 W O₂ RIE plasma for 60 s at 100 Pa, and then they were subsequently processed by 2000 W N₂ MW radical for 30 s at 100 Pa. Figure 6(a) shows the I – V characteristics of the sequentially plasma activated p-Si/p-Si bonded interface before and after annealing at 200, 400, and 600 °C for 4 h in air. The I – V measurements were repeated three times and the average values are given in figure 6(a). The measurement errors associated with this experiment were $\pm 10\%$. The barrier height shown in figure 6(b) at the bonded interface was estimated using equation (3). The I – V characteristics show that the current density reduces remarkably after annealing at 200 °C. The subsequent annealing steps at 400 and 600 °C enhance the current density. The interfacial behavior can be explained with the discrepant behavior of charges and trap densities at different temperatures.

As previously mentioned, the plasma induced charges as well as the OH⁻ groups and the incomplete nitridation

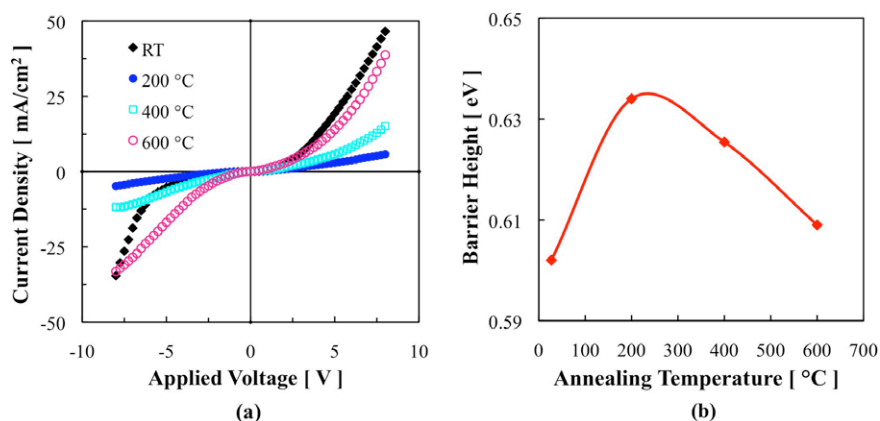


Figure 6. (a) Current–voltage characteristics of a sequentially plasma activated p-Si/p-Si bonded interface at RT and after annealing at 200, 400 and 600 °C for 4 h in air. (b) Barrier height as a function of post-bonding annealing temperature.

reactions between nitrogen plasma and silicon can be attributed to the highest current density without annealing. This incomplete nitridation acts as trapping centers.

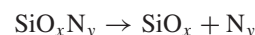
Annealing at 200 °C, we observed that some of the OH⁻ groups diffuse from the interface, expand into the bulk silicon, and increase the number of traps at the interface. The increased number of traps reduce the interface current density, resulting in increased barrier height at 200 °C. Further annealing at 400 and 600 °C, we observed that the OH⁻ desorbed from the bulk silicon, which decreased the barrier height [40]. The barrier height estimation in figure 6(b) is somewhat higher than the actual value due to the contact resistance between silver paste and silicon. However, for this comparative study, this additional contribution can be ignored. It is worth mentioning that since nitrogen atoms are not accelerated by dc bias, they cannot penetrate the silicon lattice and act as a dopant. On the other hand, oxygen atoms are accelerated by dc bias and hence can reside in a shallow surface layer (1–2 nm) and act as a dopant [39].

3.3. Nano-interface observation

To clarify the observed electrical behavior of the interface before and after annealing, we performed HRTEM of the bonded specimens. Four 2 × 2 mm² specimens were used. The first specimen did not go through any annealing steps. The three remaining specimens were each heated at an annealing temperature of 200 °C, followed by the two remaining specimens at 400 °C and the last specimen at 600 °C annealing. At all three temperatures the specimens were annealed for 4 h in air with a ramping rate of 200 °C h⁻¹. With each point of temperature increase, one new specimen was removed for observation. For the sequential activation, the wafer surfaces were processed using the parameters utilized for the experiments as shown in figure 6. Figure 7 shows the HRTEM images of p-Si/p-Si sequential plasma activated bonded interfaces. The HRTEM images show the presence of an intermediate amorphous layer at the bonded interface. The specimen which did not undergo annealing has an interface amorphous layer thickness of ~4.8 nm. The HRTEM images show that the amorphous layer thickness

remains constant at ~4.8 nm after annealing at 200 and 400 °C. However, the specimen annealed at 600 °C has an amorphous layer of ~13 nm thickness. While the amorphous layer remained constant up to 400 °C, the interface current density significantly reduced (figure 6(a)) after annealing at 200 °C. Then the current density increased at 400 and 600 °C, but the amorphous layers thickness increased at 600 °C. Therefore, no relationship was found between the amorphous layer thickness and the *I*–*V* characteristics (figure 6(a)) of the bonded interfaces at different annealing temperatures.

The abrupt change in the amorphous layer at 600 °C can be correlated with the abrupt change in void density observed from IR transmission images [40]. It has been reported that the void density of the sequentially plasma activated p-Si/p-Si bonded interface does not change with annealing up to 400 °C. The void density significantly increases after annealing at 600 °C [40]. At 600 °C, two concurrent phenomena: (1) the breaking of SiO_xN_y and (2) viscous flow of H₂ gas generated from adsorbed H₂O from bulk silicon, are responsible for the sudden increase in amorphous layer thickness. The following two reactions occur at 600 °C that increase the interfacial silicon oxide layers [40]:



These reactions produce nitrogen and hydrogen gases at the bonded interface. Since the amount of nitrogen was reported to be negligible on the sequentially treated surface [24], viscous flow of hydrogen gas may have had a dominant role as regards the increased thickness of the amorphous layers. The additional contribution to the increased thickness can be attributed to the diffusion of oxygen interstitials from bulk silicon to the interface because of the high concentration of oxygen interstitials in CZ silicon [41]. To investigate the influence of annealing ambient, a pair of bonded specimens was annealed in air and an inert gas like N₂. From IR transmission images, it was revealed that the abrupt change in void density and hence the oxide thickness at 600 °C is not influenced by the annealing ambient, but by the absorbed interface species [42].

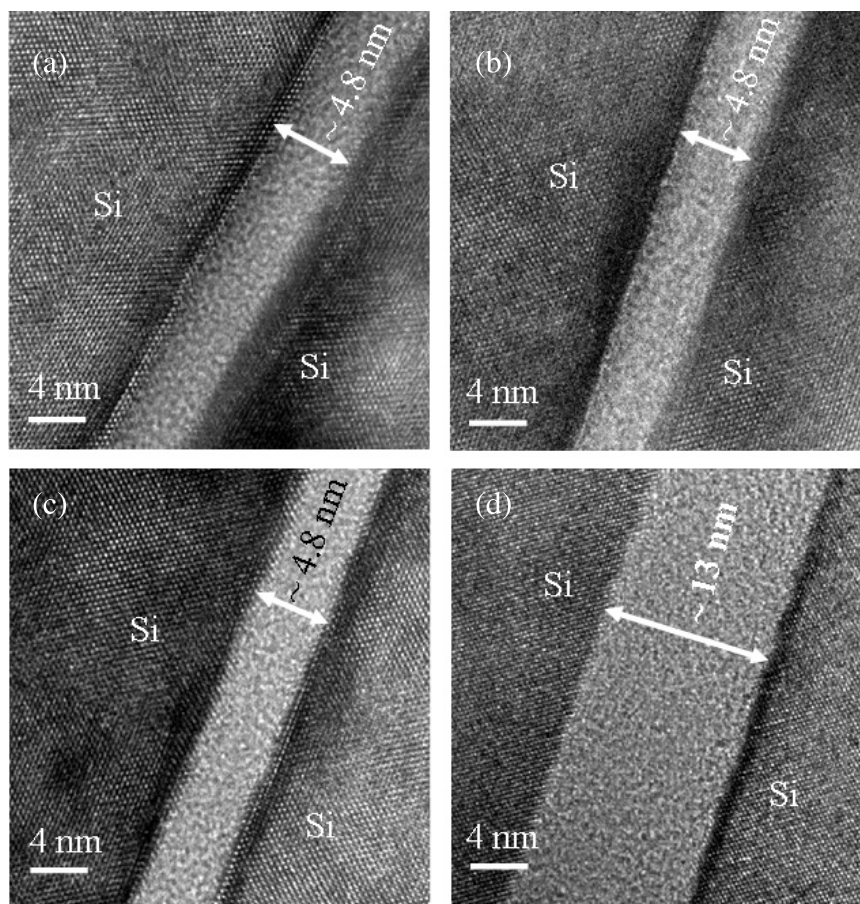


Figure 7. HRTEM images of p-Si/p-Si sequential plasma activated bonded interfaces of (a) the specimen without annealing, (b) the specimen annealed at 200 °C, (c) the specimen annealed at 400 °C, (d) the specimen annealed at 600 °C.

3.4. Compositions at the nano-interface

To investigate the elemental composition at the bonded interface, high angle annular dark-field (HAADF) scanning TEM (STEM), and electron energy loss spectroscopy (EELS) were performed with the specimen shown in figure 7(d). The EELS experiment was performed using a field-emission TEM (JEOL 2100F, $C_s = 0.50$ mm) in conjunction with a Gatan Enfina 1000 spectrometer, operating at 200 kV. The energy resolution was about 1.0 eV. Typical probe conditions for EELS used in this work consisted of a 1.0 nm diameter probe in the TEM condition and a ~ 0.3 nm diameter probe with a convergence semi-angle of 14 mrad in the STEM condition. Core loss EELS spectra of N K, Si $L_{2,3}$, and O K were recorded.

Figure 8 shows (a) the STEM image of the bonded interface, (b) the EELS for detection of elements at the interface. The STEM image shows an ~ 13 nm interfacial amorphous layer at the bonded interface. From the EELS spectra, no nitrogen was detected at the bonded interface. Both the Si $L_{2,3}$ edges at 125–175 eV and the O K edges at 540–560 eV were observed at amorphous oxide layers of the interface. A further analysis of the Si $L_{2,3}$ of amorphous Si oxide compared with Si and SiO_2 provides the characteristic behavior of amorphous layers at the interface. Figure 8(b) shows the Si $L_{2,3}$ edges from the interfacial amorphous oxide

layer compared with the standard Si and SiO_2 . The Si $L_{2,3}$ edges from the amorphous layer were identical to those of the standard SiO_2 at the bonded interface. This implies that SiO_2 is present at the interface. This is because of the annealing of the specimen at 200, 400 and 600 °C for 4 h at each step in air.

4. Conclusions

Sequential plasma activated bonding (SPAB) of silicon wafers has been studied to facilitate the spontaneous bonding required for nanostructure integration on the wafer scale. The sequential activation offers highly reactive and hydrophilic surfaces compared to those of non-activated and hydrofluoric acid treated surfaces due to the high reactivity of N_2 MW radicals. The I – V measurements show that the current transport across the nanobonded interface can be improved by decreasing the O_2 RIE activation time. HRTEM images confirm the nanometer scale bonding of the mating wafers with an interface amorphous layer thickness of 4.8 nm. EELS results reveal the presence of SiO_2 at the nanobonded interface. Our investigations show that the proper choice of plasma parameters can offer a highly reactive surface associated with improved current transport which is required for spontaneous integration of nanostructures at room temperature. Further

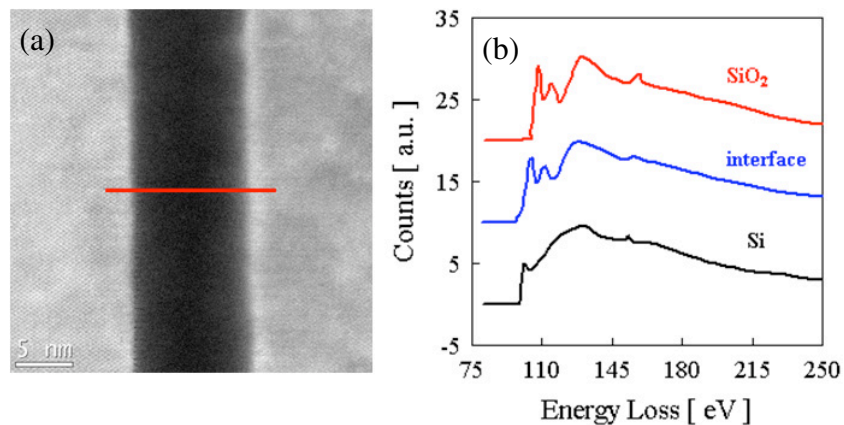


Figure 8. (a) STEM image of the bonded interface of the specimen shown in figure 7(d); (b) compositional distribution along the red line shown in (a) by the EELS analysis.

research is ongoing, to realize the spontaneous integration of nanostructures on the wafer scale.

Acknowledgments

This research was supported by a discovery grant (No. 327947) from the Natural Science and Engineering Research Council of Canada and an infrastructure grant (No. 12128) from the Canada Foundation for Innovation (CFI). Professor Jamal Deen is greatly thanked for his support and assistance in establishing nanobonding and interconnection research at the Micro- and Nano-Systems Laboratory at McMaster University. The authors acknowledge Professor Tadatomo Suga for the development of the sequentially plasma activated bonding method. Dr J G Wang of the University of Texas at Dallas is thanked for his assistance in the EELS observations. A Yamauchi of Bondtech Corporation and G Kagami of Shinko Seiki Co. Ltd, Japan, are acknowledged for their assistance in the construction of the hybrid plasma bonding system.

References

- [1] Tong Q Y and Gösele U 1999 *Semiconductor Wafer Bonding: Science and Technology* (New York: Wiley)
- [2] Morris J E 2008 *Nanopackaging, Nanotechnology and Electronics Packaging* (Berlin: Springer)
- [3] Christiansen H, Singh R and Gösele U 2006 *Proc. IEEE* **94** 2060
- [4] Lu S, Liu Y, Shao N and Panchapakesan B 2007 *Nanotechnology* **18** 065501
- [5] Aradhya S V, Garimella S V and Fisher T S 2008 *J. Electrochem. Soc.* **155** 161–5
- [6] Gu Z, Ye H, Bernfeld A, Livi K J T and Gracias D H 2007 *Langmuir* **23** 979
- [7] Gu Z, Ye H, Gracias D H and Gracias D 2005 *J. Miner. Metals Mater. Soc.* **57** 60
- [8] Chen C, Yan L, Kong S-W and Zhang Y 2006 *Nanotechnology* **17** 2192
- [9] Johnson R D, Bahr D F, Richards C D, Richards R F, McClain D, Green J and Jiao J 2009 *Nanotechnology* **20** 065703
- [10] Arokiaraj J, Tripathy S, Vicknesh S and Chua S J 2006 *Appl. Surf. Sci.* **253** 1243
- [11] Howlader M M R, Suehara S, Takagi H, Kim T H, Maeda R and Suga T 2006 *IEEE Trans. Adv. Packag.* **29** 446
- [12] Sanz-Velasco A, Amirfeiz P, Bengtsson S and Colinge C 2003 *J. Electrochem. Soc.* **150** G155
- [13] Li H, Zheng Y, Akin D and Bashir R 2005 *J. Micrielectromech. Syst.* **114** 103–12
- [14] Islam M S, Sharma S, Kamins T I and Williams R S 2004 *Nanotechnology* **15** L5–8
- [15] Lyer S S and Auberton-Herve A J 2002 *Silicon Wafer Bonding Technology for VLSI and MEMS Applications* (London: INSPEC)
- [16] Wagener M C, Zhang R H, Rozgonyi G A, Seacrist M and Ries M 2007 *Appl. Phys. Lett.* **90** 112101
- [17] Bengtsson S and Engstrom O 1989 *J. Appl. Phys.* **66** 1231
- [18] Amirfeiz P, Bengtsson S, Berg M, Zanghellini E and Borjesson L 2000 *J. Electrochem. Soc.* **147** 2693
- [19] Raeissi B, Sanz-Velasco A and Engstrom O 2006 *ECS Trans.* **3** 217
- [20] Prabhakaran K and Ogino T 1999 *Bull. Mater. Sci.* **22** 553
- [21] Kanno I, Yamashita M, Nomiya S and Onabe H 2006 *Japan. J. Appl. Phys.* **45** 7938
- [22] Ma X, Chen C, Liu W, Liu X, Du X, Song Z and Lin C 2009 *J. Electrochem. Soc.* **156** H307
- [23] Young T 1805 *Phil. Trans. R. Soc. London* **9** 255
- [24] Howlader M M R, Suga T, Itoh H and Kim M J 2006 *ECS Trans.* **3** 191
- [25] Yang C, Tartaglino U and Persson B N J 2006 *Phys. Rev. Lett.* **97** 116103
- [26] Choi S-W, Choi W-B, Lee Y-H, Ju B-K, Sang M-Y and Kim B-H 2002 *J. Electrochem. Soc.* **149** G8
- [27] Howlader M M R, Suga T, Itoh H, Lee T H and Kim M J 2009 *J. Electrochem. Soc.* **156** H846
- [28] Suga T, Kim T H and Howlader M M R 2004 *54th Electronic Comp. and Tech. Conf.* vol 1, p 484
- [29] Good R J 1992 *J. Adhes. Sci. Technol.* **6** 1269
- [30] Wan G J, Fu R K Y, Yang P, Ho J P Y, Xie X, Huang N and Chu P K 2006 *Nucl. Instrum. Methods Phys. Res. B* **242** 296
- [31] Wang C, Higurashi E and Suga T 2008 *Japan. J. Appl. Phys.* **47** 2526
- [32] Zhou Y C, Zhu Z H, Crouse D and Lo Y H 1998 *Appl. Phys. Lett.* **73** 2337
- [33] Pasquariello D, Hedlund C and Hjort K 2000 *J. Electrochem. Soc.* **147** 2699
- [34] Bengtsson S and Engstrom O 1991 *Japan. J. Appl. Phys.* **30** 356
- [35] Henriksen K S, Taklo M M V, Hanneborg A and Jensen G U 2002 *Sensors Actuators A* **102** 99
- [36] Sze S M 1981 *Physics of Semiconductor Devices* 2nd edn (New York: Wiley)

- [37] Wagener M C, Zhang R H and Rozgonyi G A 2007 *Appl. Phys. Lett.* **90** 112101
- [38] Bos J and Hendriks M 1989 *J. Appl. Phys.* **66** 1244
- [39] Suni T, Henttinen K, Suni I and Mäkinen J 2002 *J. Electrochem. Soc.* **149** G348
- [40] Howlader M M R *et al* 2009 *J. Microelectromech. Syst.* submitted
- [41] Ahn K-Y, Stengl R, Tan T Y and Gösele U 1989 *J. Appl. Phys.* **65** 561
- [42] Howlader M M R, Kibria M G, Zhang F and Kim M J 2009 *J. Electrochem. Soc.* to be submitted